Formally, this generalized form of P is expressed as:

$$P_\mu = (k_\mu, \tilde{n}_\mu) = \left(\pi \cdot \sqrt{\frac{\rho_1^2 - \rho_0^2}{n_1^2 - n_0^2}}\ , \sqrt{\frac{n_1^2 - n_0^2 \eta^2}{1 - \eta^2}} \right), \tag{5}$$

where $\rho_i = m_{i\mu}/t_i$ $(i = 1,0)$ and $\eta = \rho_1/\rho_0$. The parametrized phase orders are defined here as $m_{1\mu} = m_1 - \mu$ and $m_{0\mu} = m_0 + \mu$ with $m_i \in \mathbb{Z}^+$ and $\mu \in \mathbb{R}^+$, representing (via μ) arbitrary phase accumulation within the high- and low-index layers, respectively. The addition of the accumulated phases in each layer thus produces a constant value $\phi_1 + \phi_0 = (m_{1\mu} + m_{0\mu})\pi = (m_1 + m_0)\pi = \pi, 2\pi, \ldots = \text{const.}\ \forall\ (k, \tilde{n})$ on P_μ, as asserted above. Note that this expression is simple in that it returns the k along P_μ at an effective index $\tilde{n}$ given only the values of the layer properties t_i and n_i, the order of the bandgap of interest $\langle m_1, m_0 \rangle$ (cf. Ref. [18]) and the parametric order value μ which effectively determines the position along the P_μ curve. In practice, this expression can be easily evaluated over a range of μ to define a curve through a given gap over $(\lambda, \tilde{n})$ as shown in Fig. 5.

The form of P_μ is identical to P defined in Ref. [18] except that the orders $m_{i\mu}$ are generalized to be continuous ($\mu \in \mathbb{R}^+$) instead of discrete integers or half integers ($\mu = 0$ or $1/2$), representing arbitrary phase accumulation within each layer instead of just resonance and antiresonance, respectively. The integer terms $m_i \in \mathbb{Z}^+$ correspond, via P_μ, to the local bound region of order $\langle m_1, m_0 \rangle$ (a nomenclature suggested previously [18]). In this way, given a specific bound region $\langle m_1, m_0 \rangle$, P_μ traces out a curve within the region for $\mu = 0 \to 1$, starting at the maximal bounding point P_0 [P_μ of order (m_1, m_0)], passing through the central point $P_{1/2}$ [P_μ of order $(m_1 - 1/2, m_0 + 1/2)$] and finishing at the minimal bounding point P_1 [P_μ of order $(m_1 - 1, m_0 + 1)$].

In other words, when compared to Bloch bandgap spectra, the curve swept out by P_μ for varying μ passes through the closure points (P_0 and P_1) and the approximate central point ($P_{1/2}$) of an arbitrary bandgap (when these points exist in the domain $0 \leq \tilde{n} \leq n_0$ for a given bound region $\langle m_1, m_0 \rangle$). P_μ thus provides an approximation to the central λ or k of a given bandgap for arbitrary $\tilde{n}$ within the gap. Like the SPARROW model it is inherited from, this generalized central curve definition holds for any alteration in $\tilde{n}$ (or k), such as when the core size or shape is altered, higher-order modes are considered or when, as for the case here, the core refractive index of a Bragg waveguide is changed directly.

In the cases considered here, when compared to the calculated Bloch bandgap center k_c^{Bloch} [Eq. (2)], when ignoring material dispersion, P_μ provides an agreement to better than 0.5% for the TM bandgap and 4% for the TE bandgap central wavelengths for all core refractive indices considered. The agreement is shown in Fig. 5 (*top*) where the P_μ curves appear to lie on top of the calculated Bloch bandgap center curves (λ_c^{Bloch}). The dispersive layer index case (Fig. 5, *bottom*) produces slightly larger wavelength differences of 0.8% and 5% for the TM and TE gaps, respectively. In both cases, the TE gap center begins to deviate for higher $\tilde{n}$ due to the fact that P_μ appears to intercept the TM gap closure point (P_B, due to the Brewster effect [3, 18, 25], as above) which doesn't coincide with the TE gap center. Also, the P_μ approximation to the gap center breaks down as $\tilde{n} \to n_0$ for gaps terminating on the low-index line $\tilde{n} = n_0$, where $k_c^{\text{res.}}$ [Eq. (4)] and other simple expressions provide a better approximation, *e.g.*, Ref. [27]; these latter points will be discussed in future work.

Given the close agreement between P_μ and the Bloch bandgap center, P_μ also shows a reasonable agreement with the experimentally measured transmission peak positions, compared directly in Fig. 4.

4.1. *Sensitivity to refractive index*

An analytic expression for the sensitivity of λ to changes in $\tilde{n}$ along the P_μ curve is now derived, extending the theory developed above. For large core waveguides, where $\tilde{n} \approx n_{\text{core}}$, this is thus a measure of the sensitivity of the transmission peak central wavelength to changes in the core index. As for the definition of P_μ, this treatment is applicable to arbitrary bandgaps of arbitrary binary stacks (waveguide or otherwise). Using this general expression, an example is given based on the fundamental bandgap of the Bragg fiber cladding structure considered above.

Given that Eq. (5) is analytic, one can derive a closed form for the partial derivative of $\tilde{n}_\mu$ versus the wavenumber k_μ (hence frequency or wavelength): $\partial\tilde{n}_\mu/\partial k_\mu$. The inverse of this, $\partial k_\mu/\partial\tilde{n}_\mu$, is thus a measure of the sensitivity of a bandgap center to changes in the effective refractive index of the guided light. Note that this closed form derivation assumes the refractive indices are locally flat over the spectrum, *i.e.*, at a wavelength λ', the index takes value $n_i(\lambda) = n_i(\lambda')$ according to it's material dispersion (*e.g.*, Fig. 2) but one assumes $\partial n_i/\partial\lambda = 0$. Later, this approximation is compared to the full numerical derivative which inherently includes the material dispersion derivative ($\partial n_i/\partial\lambda \neq 0$). The approximate closed form of the sensitivity is now derived.

The coordinates of the $P_\mu = (k_\mu, \tilde{n}_\mu)$ curve are related via the parameter μ. In general, then:

$$\frac{\partial\tilde{n}_\mu}{\partial k_\mu} = \frac{\partial\tilde{n}_\mu}{\partial\eta}\cdot\frac{\partial\eta}{\partial\mu}\cdot\frac{\partial\mu}{\partial k_\mu} = \frac{\partial\tilde{n}_\mu}{\partial\eta}\cdot\frac{\partial\eta}{\partial\mu}\Big/\frac{\partial k_\mu}{\partial\mu}, \tag{6}$$

where the final step results from the parametric nature of the relationship between $\tilde{n}_\mu$ and k_μ. From Eq. (5):

$$\frac{\partial\tilde{n}_\mu}{\partial\eta} = \frac{\eta}{1-\eta^2}\frac{n_0^2-\tilde{n}_\mu^2}{\tilde{n}_\mu}, \tag{7}$$

and note that:

$$\frac{\partial\eta}{\partial\mu} = -\frac{t_0+t_1\eta}{(m_0+\mu)t_1}. \tag{8}$$

Similarly, from Eq. (5):

$$\frac{\partial k_\mu}{\partial\mu} = -\frac{\pi^2}{(n_1^2-n_0^2)k_\mu}\left(\frac{m_1-\mu}{t_1^2}+\frac{m_0+\mu}{t_0^2}\right). \tag{9}$$

Combining these via Eq. (6) and inverting the numerator and denominator:

$$\frac{\partial k_\mu}{\partial\tilde{n}_\mu} = \pi^2\frac{1-\eta^2}{(n_1^2-n_0^2)\eta}\frac{(m_0+\mu)t_1}{t_0+t_1\eta}\left(\frac{m_1-\mu}{t_1^2}+\frac{m_0+\mu}{t_0^2}\right)\frac{\tilde{n}_\mu}{(n_0^2-\tilde{n}_\mu^2)k_\mu}. \tag{10}$$

Defining $\lambda_\mu = 2\pi/k_\mu$, implying $\partial k_\mu = -(k_\mu^2/2\pi)\partial\lambda$, Eq. (10) can be expressed in terms of wavelength as:

$$\begin{aligned}\frac{\partial\lambda_\mu}{\partial\tilde{n}_\mu} &= \frac{2\pi}{k_\mu^2}\frac{\partial k_\mu}{\partial\tilde{n}_\mu}\\ &= -2\pi^3\frac{1-\eta^2}{(n_1^2-n_0^2)\eta}\frac{(m_0+\mu)t_1}{t_0+t_1\eta}\left(\frac{m_1-\mu}{t_1^2}+\frac{m_0+\mu}{t_0^2}\right)\frac{\tilde{n}_\mu}{(n_0^2-\tilde{n}_\mu^2)k_\mu^3}.\end{aligned} \tag{11}$$

Equation (11) thus describes the sensitivity of the λ_μ component of the P_μ point for changes in $\tilde{n}_\mu$ [as does Eq. (10) for the sensitivity of k_μ]. It thus also provides an approximation to

#156491 - $15.00 USD Received 14 Oct 2011; revised 25 Nov 2011; accepted 28 Nov 2011; published 19 Dec 2011

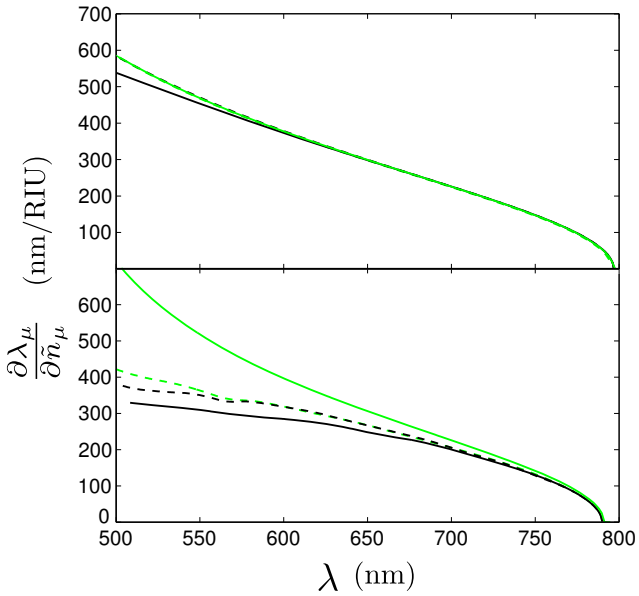

Fig. 6. Sensitivity of the exact and approximate center of the fundamental bandgap to changes in $\tilde{n}$ for the layer properties described in § 2. *Top*: without material dispersion [$n_i = n_i(\lambda = 700\text{ nm})$]. *Bottom*: with material dispersion [$n_i = n_i(\lambda)$]. *Black*: numerically calculated sensitivity of the Bloch bandgap center [from k_c^{Bloch}, Eq. (2)]; *solid*: TE; *dashed*: TM. *Green*: the wavelength sensitivity of the P_μ point in to changes in $\tilde{n}$; *solid*: analytic approximation to derivative of P_μ neglecting material dispersion derivatives [Eq. (11) – setting $\partial n_i/\partial\lambda = 0$ but allowing $n_i = n_i(\lambda)$]; *dashed*: numerical derivative of P_μ including material dispersion [$\partial n_i/\partial\lambda \neq 0$].

the sensitivity of an arbitrary Bloch bandgap center to changes in $\tilde{n}$. In the large-core regime here where $\tilde{n} \approx n_{\text{core}}$, this is thus an approximation to the sensitivity of the Bloch bandgap center (and hence waveguide transmission peak) to changes in the core refractive index. This expression for the sensitivity can be evaluated for any given point (any value of μ) on the central curve $P_\mu = (k_\mu, \tilde{n}_\mu)$ and obviates the need for numerical derivation of P_μ or k_c^{Bloch} over $(k, \tilde{n})$ (keeping in mind the approximation of locally flat material dispersion: $\partial n_i/\partial\lambda = 0$).

For the case of non-dispersive layer materials, where $n_i = \text{const.}$, Eq. (11) provides an excellent approximation to the Bloch bandgap sensitivity $\partial\lambda_c^{\text{Bloch}}/\partial\tilde{n}$ (where $\lambda_c^{\text{Bloch}} = 2\pi/k_c^{\text{Bloch}}$). Figure 6 (*top*) demonstrates this for the Bragg fiber considered above. The Bloch gap sensitivity is calculated numerically, directly from k_c^{Bloch} [Eq. (2)]. Due to the good agreement between P_μ and k_c^{Bloch} (Fig. 5), there is an excellent agreement between their derivatives: the TM gap sensitivity agrees to better than 0.5% and the TE to better than 8.5% for all wavelengths considered.

While Eq. (11) doesn't explicitly include material dispersion [dispersive indices $n_i = n_i(\lambda)$ are permitted but $\partial n_i/\partial\lambda = 0$ is enforced] it can be used as a reasonable analytic approximation to the Bloch bandgap center sensitivity when material dispersion cannot be neglected, demonstrated in Fig. 6 (*bottom*). In this case, k_μ and $\tilde{n}_\mu$ are calculated from Eq. (5) via root-finding and used to evaluate Eq. (11) directly, *i.e.*, P_μ is evaluated with material dispersion, but the evaluation of the derivative assumes the dispersion of the layer indices is locally flat ($\partial n_i/\partial\lambda = 0$). The agreement deviates significantly toward shorter wavelengths as may be expected – this is the region where the material indices fluctuate most (cf. Fig. 2) – but is still within 50% of the TM Bloch gap sensitivity for $\lambda \approx$570 nm, and much better for longer λ.

The complete inclusion of material dispersion ($\partial n_i/\partial\lambda \neq 0$) results in more complex expres-

#156491 - $15.00 USD Received 14 Oct 2011; revised 25 Nov 2011; accepted 28 Nov 2011; published 19 Dec 2011

sions. One straightforward alternative is to use numerical root-finding of the P_μ coordinates (as above) but then also numerically calculate the local slope, rather than approximating it analytically as per Eq. (11); this inherently includes the spectral derivatives of the layer materials but requires a significant number of calculated points, and hence iterations, for sufficient precision. The evaluation of the Bloch gap sensitivity in Fig. 6 was also calculated numerically in this fashion and hence also inherently includes the full material dispersion. Figure 6 (*bottom*) shows the comparison between these numerical derivatives of P_μ and the Bloch bandgap central wavelength when the layers' material dispersion is considered. As expected from their good agreement in absolute value as per Fig. 5, their sensitivities also agree well: below 1% for $\lambda \gtrsim 575$ nm and better than 9.5% over all wavelengths considered for the TM gap centre.

The numerical derivatives of the Bloch center and P_μ (both including material dispersion) agree well with experiment. From four data points, the experimental results implied an approximately linear sensitivity of 330 nm/RIU, § 2. As Fig. 6 shows, from a continuous range of points over the wavelengths of interest (λ=700 nm–500 nm), the numerical calculations predict sensitivities of $\partial\lambda_c^{\text{Bloch}}/\partial\tilde{n} \approx$ 200–383 nm/RIU and $\partial\lambda_\mu/\partial\tilde{n} \approx$ 200–422 nm/RIU. The analytical approximation of the latter [Eq. (11)] agrees well with these values for longer wavelengths but deviates, increasing to ≈719 nm/RIU at λ=500 nm, due to the appreciable material dispersion at shorter λ (Fig. 2). In regimes of non-negligible dispersion, Eq. (11) is thus useful as a rapid design tool, with the full numerical values required for more precise calculations.

4.2. Sensitivity trends

The analytical form of P_μ [Eq. (5)] and hence $\partial\lambda_\mu/\partial\tilde{n}$ [Eq. (11)] allows some fundamental physical observations to be made with respect to the sensitivity. The case considered here has layers of a high refractive index contrast. The $1/(n_1^2 - n_0^2)$ dependence of $\partial\lambda_\mu/\partial\tilde{n}_\mu$ implies that layers with a lower refractive index contrast would produce a more sensitive response to $\tilde{n}$ (core index here). Also, the $1/(\tilde{n}^2 - n_0^2)$ dependence of Eq. (11) implies that $\tilde{n}$ variations closer to the low layer index ($\tilde{n} = n_0$) will induce more sensitive spectral shifts. One can see from Fig. 5, for example, that this is the case since the gaps generally flatten out as $\tilde{n} \to n_0$ over $(\lambda, \tilde{n})$, and is demonstrated explicitly by the sensitivity curves of Fig. 6.

This suggests that Bragg waveguides with a low contrast between the cladding layer refractive indices should be more sensitive to changes in the core index than those with a high contrast, especially when the core refractive index is also close to the lowest of the cladding layer indices. Indeed, this has recently been shown experimentally by Qu and Skorobogatiy [27] who demonstrated refractive index sensing with sensitivities of ≈ 1400 nm/RIU in aqueous solutions via a polymer Bragg fiber made from low-index polymers with a low refractive index contrast. The low refractive index values of the cladding layers and their low contrast with each other allowed this regime of increased sensitivity to be reached, as just discussed. Indeed, such polymers are possibly the only presently practical materials with which low contrast with aqueous solutions could be achieved within a hollow Bragg waveguide.

Alternatively, these identified trends can be used in reverse to design structures that are almost invariant to changes in the core index: high index contrast layers and/or core indices far from the layer indices. This would be useful in scenarios in which a sample's refractive index might fluctuate but a constant guided spectrum is desired.

Note that the theory and results developed and used here are applicable to layers of *arbitrary* refractive index, not just to the regime of low index contrast, say. It is thus useful as an analysis and design tool for many platforms and devices of interest today with arbitrary layer indices (of high or low contrast) and arbitrary core (n_{core}) or effective mode indices ($\tilde{n}$) – up to the aforementioned $\tilde{n} \to n_0$ approximation limit (§ 4) – such as most modern hollow Bragg fibers and I-ARROWs that can be filled with liquids.

#156491 - $15.00 USD Received 14 Oct 2011; revised 25 Nov 2011; accepted 28 Nov 2011; published 19 Dec 2011

5. Discussion and conclusion

The shifting of the transmission spectrum of a Bragg fiber with high cladding layer index contrast has been experimentally demonstrated by filling the hollow core with liquids of various refractive indices. An analytical model was derived to describe the spectral behaviour of such binary layered systems and was compared to the experimental results.

The Bragg fiber used in this work demonstrated a transmission peak sensitivity to core refractive index of $\partial\lambda_{\text{peak}}/\partial n_{\text{core}} \approx 330$ nm/RIU, which is comparable with the results of a similar I-ARROW based architecture (which relies on detection of a transmission minimum, not maximum as used here) [8]. This sensitivity is lower than the low index contrast Bragg fiber sensor demonstrated by Qu and Skorobogatiy [27], but the cladding layer index contrast here is much higher, producing a larger dynamic range in core index aided by the omnidirectional nature of the bandgap; the main purpose of the results presented here was to analyse the response of binary layered systems to light of arbitrary effective indices, in both theory and experiment, rather than the optimum design of a sensor device.

Reasonable agreement with what is expected from a Bloch wave based analysis was achieved, but only when the material dispersion of the layers was incorporated since the layer materials demonstrate non-negligible dispersion over the wavelength range of interest. The layers' material dispersion acted in such a way that the band edges 'straightened out' compared to the equivalent bandgap spectrum in the absence of material dispersion. This material-induced band edge straightening was verified both in experiment (by the approximate linearity of the peak shifting with core index, § 2) and theory (by calculation of the bandgap maps and centers incorporating the material dispersion, § 4).

A novel theory was developed, defining a simple analytic expression for P_μ [Eq. (5)]: a generalized, parametric, version of the intersection point P of the SPARROW model [18]. The expression is simple in that it requires only the input of the layer parameters n_i and t_i and the bandgap/resonance order $\langle m_1, m_0 \rangle$ of interest. P_μ was shown to be a close approximation to the central frequency of the considered bandgap spectra. For the Bragg fiber cladding considered here, P_μ approximated the TM Bloch bandgap central wavelength to better than 0.8% for all cases considered. For large core waveguides (where $\tilde{n} \approx n_{\text{core}}$), this analytic expression can be used to analyse and design binary layer waveguides with low-index cores for arbitrary layer parameters, core indices, and bandgaps/resonances.

The analyticity of P_μ allowed an analytic expression for its derivative to be found ($\partial\lambda_\mu/\partial\tilde{n}_\mu$), thus describing the sensitivity of the approximate bandgap central frequency to changes in the effective index $\tilde{n}$ (by altering the core index, say). Good agreement between the analytic P_μ sensitivity and the numerically calculated Bloch bandgap center sensitivity was shown (Fig. 6). The sensitivity expressions also agreed well with the measured sensitivity of the filled Bragg fiber considered (≈ 330 nm/RIU), which included the effects of nontrivial layer material dispersion while maintaining analyticity (by assuming the layer indices, while variable with λ, are everywhere locally flat). The expression was used to show how the sensitivity could be enhanced by using low refractive index contrasts between cladding layers and/or between the core and cladding layers or, alternatively, how the sensitivity could be reduced by using high contrasts to produce devices with invariant spectral properties under fluctuating sample indices.

These results highlight some of the key features of variable core index multilayer waveguides, emphasizing the importance of low-index–core and liquid–core binary layered cladding waveguides (such as Bragg fibers or I-ARROWs) in sensing, microfluidics, fiber lasers, and novel nonlinear devices. These results can also be applied to investigations of the design and operation of other devices such as binary multilayer reflectors in general, with arbitrary incidence angle or index, and to structures with a binary cladding such as SEFLs [13] and VCSELs [15] with cores or cavities of various or varying refractive indices.

#156491 - $15.00 USD Received 14 Oct 2011; revised 25 Nov 2011; accepted 28 Nov 2011; published 19 Dec 2011